Propagation Measurements and Modeling of Crossing Bridges on High-Speed Railway at 930 MHz

Ke Guan, *Student Member, IEEE*, Zhangdui Zhong, Bo Ai, *Senior Member, IEEE*, and Thomas Kürner, *Senior Member, IEEE*

***Abstract*—Bridges that cross a railway's right-of-way are one of the most common obstacles for wave propagation along a high-speed railway. They can lead to poor coverage or handover failure but have been rarely investigated before. To describe the influence of this nonnegligible structure on propagation, measurements have been taken at 930 MHz along a real high-speed railway in China. Based on different mechanisms, the entire propagation process is presented by four zones in the case of an independent crossing bridge (ICB) and two zones in the case of groups of crossing bridges. First, all the propagation characteristics, including extra propagation loss, shadow fading, small-scale fading, and fading depth, have been measured and extracted. The results are shown in a complete table for accurate statistical modeling. Then, two empirical models, i.e., ICB and crossing bridges group (CBG), are first established to describe the extra loss owing to the crossing bridges. The proposed models improve on the state-of-the-art models for this problem, achieving a root mean square error (RMSE) of 3.0 and 3.7 dB, respectively.**

***Index Terms*—Crossing bridges, propagation loss modeling, propagation measurements, railway communications.**

I. Introduction

As ONE of the most promising means of transportation, high-speed railways have been experiencing fast development all over the world. Accurate characterization of the radio channel is the basis of signaling and train control communications systems, and therefore, it directly determines the secure operation of high-speed railways. To ensure the speed of up to 350 km/h, a gentle grade of rail is required. Hence, cuts and viaducts are largely employed to keep the rail straight. This results in a great number of crossing bridges over the track. As shown in Fig. 1(a), this kind of reinforced concrete made crossing bridges one of the most common obstacles along a high-speed railway. They indeed block line of sight (LOS) and attenuate the received signal power.

Among the works related to propagation on a high-speed railway, for the narrow-band channel, Wei *et al.* in [1] presented

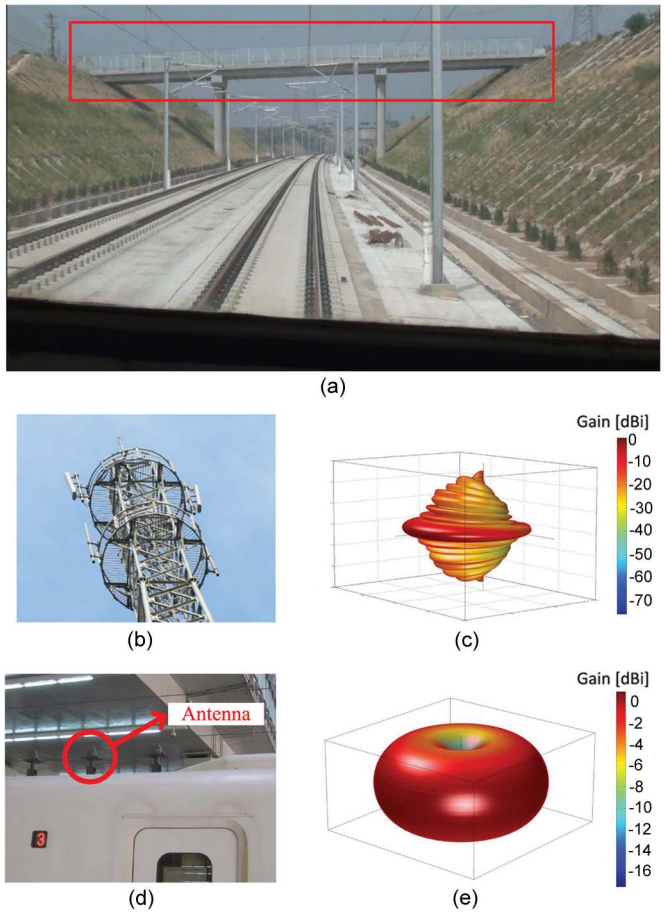

Fig. 1. (a) Typical crossing bridge in the measurements along a high-speed railway. (b) Transmitting antennas. (c) 3-D pattern of the transmitting antenna. (d) Receiving antenna, installed on top of the carriage. Only the middle antenna was used in the measurements. (e) Free-space 3-D pattern of the receiving antenna.

Manuscript received January 8, 2013; revised April 15, 2013 and June 25, 2013; accepted June 26, 2013. Date of publication August 1, 2013; date of current version February 12, 2014. This work was supported in part by the National Natural Science Foundation of China under Grant 61222105, by the Beijing Municipal Natural Science Foundation under Grant 4112048, by the Key Project of the Chinese Ministry of Education under Grant 313006, by the Project of the State Key Laboratory under Grant RCS2012ZT013, by the Fundamental Research Funds for the Central Universities under Grant 2010JBZ008, by the Key Project for the Railway Ministry of China under Grant 2012X008-A, and by the State Key Laboratory of Rail Traffic Control and Safety under Grant RCS2011K008 and Grant RCS2011ZZ008. The review of this paper was coordinated by Prof. M. D. Yacoub. *(Corresponding author: B. Ai.)*

K. Guan is with the State Key Laboratory of Rail Traffic Control and Safety, Beijing Jiaotong University, Beijing 100044, China, and also with the Institut für Nachrichtentechnik, Technische Universität Braunschweig, Braunschweig, 38106, Germany (e-mail: myecone@hotmail.com).

Z. Zhong and B. Ai are with the State Key Laboratory of Rail Traffic Control and Safety, Beijing Jiaotong University, Beijing 100044, China.

T. Kürner is with the Institut für Nachrichtentechnik, Technische Universität Braunschweig, Braunschweig, 38106, Germany.

Color versions of one or more of the figures in this paper are available online at http://ieeexplore.ieee.org.

Digital Object Identifier 10.1109/TVT.2013.2275912

empirical path loss models in a viaduct scenario and the scenario in which the track is neither in a cut nor on a viaduct. The path loss, shadow fading, and small-scale fading behavior in a cut scenario have been measured and analyzed in [2]–[5]. Briso *et al.* in [6] carried out a series of measurements at 900 MHz based on distributed antenna systems in a tunnel on a high-speed rail in Spain. A set of measurements conducted at 2.4 GHz in a realistic tunnel environment was presented in [7]. In [8]–[11], Guan *et al.* described the propagation channel in the near-region of rectangular, circular, arched, and arbitrary cross-sectional tunnels by analytically modeling the dividing point between different propagation mechanisms. The propagation characteristics of break-point, near-zone, and far-zone inside tunnels were researched in [12]. Based on the measurement, the near-shadowing phenomenon inside tunnels were observed and modeled in [13]. Guan *et al.* in [14]–[17] presented hybrid models inside tunnels covering various propagation mechanisms with two types of users.

For the wideband system, in [18], Liu *et al.* analyzed the propagation mechanisms and established a position-based channel model from experimental results for the viaduct scenario. The Long-Term Evolution for Railway (LTE-R) was assessed by using a hybrid high-speed railway channel model in [19]. Moreover, some deterministic approaches for wave propagation modeling in a high-speed railway based on the ray-launching method were presented in [20]–[23]. However, the propagation influence of crossing bridges has been rarely investigated before. Only Lu *et al.* in [24] mentioned that there is a need to perform a quantitative analysis of the propagation loss caused by crossing bridges. However, the subsequent in-depth investigation is still absent.

This limitation leads to the following open questions to the wireless planners and system designers.

- What is the influence of crossing bridges on the wireless channel? How can shadow fading and small-scale fading be characterized in the regions under or behind the crossing bridge?
- What is the range of the influence of a crossing bridge? Are there any correlations among neighboring crossing bridges, or are there any differences if the crossing bridges are far from each other or near each other?
- How severe is the extra loss that comes from a crossing bridge? Can the traditional multiedge models still work for the case of a crossing bridge? If not, how can this extra loss be predicted in network planning?

To answer these questions, in this paper, the narrow-band propagation characteristics in the related region of crossing bridges at 930 MHz are measured and extracted. Moreover, two empirical models for the extra propagation loss are presented.

According to the correlation of the influence of crossing bridges, two basic cases can be classified, i.e., independent crossing bridge (ICB) and crossing bridges group (CBG). Based on different propagation mechanisms, the entire process of the case of ICB is separated into four zones, and the process in CBGs is divided into two zones. By employing extensive measured data collected along a real high-speed railway, we present a detailed statistical analysis of channel parameters and empirical modeling for the extra propagation loss. The accurate measurement, statistical analysis, and empirical models for each zone of each case fill the gap of current high-speed railway modeling, making the design of train control systems able to meet the realistic condition.

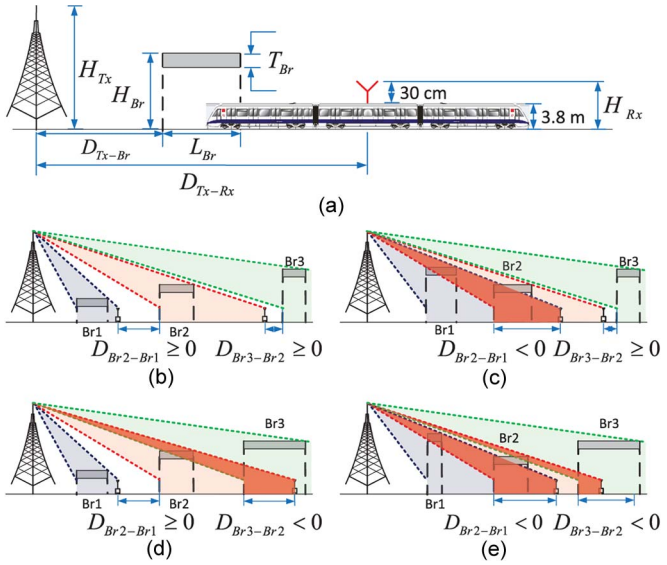

Fig. 2. (a) Measurement scenarios. (b) ICB 1, 2, and 3. (c) Related crossing bridge 1 and 2, but independent 3. (d) ICB 1, but related 2 and 3. (e) Related crossing bridge 1, 2, and 3. The different sizes and heights of the bridge schematics are used to show how the related regions appear when the dimensions of crossing bridges change.

This paper is organized as follows. Some definitions related to crossing bridges are given in Section II. Section III describes the measurement campaign. Section IV provides a detailed statistical analysis of channel parameters. Section V presents two empirical models for the extra propagation loss resulting from the ICB and the CBG, respectively. Validations and comparisons with the classic models and measured data are provided as well. In Section VI, conclusions are drawn.

II. Definitions Related to Crossing Bridges

A. Geometrical Parameters of Crossing-Bridge Scenarios

Fig. 2(a) shows a sketch of the crossing-bridge scenarios, including the following geometrical parameters.

- H_{Tx}, H_{Rx}, and H_{Br} are the heights of the transmitter (Tx), the receiver (Rx), and the crossing bridge relative to the track, respectively.
- T_{Br}, L_{Br}, and $D_{\mathrm{Tx-Br}}$ are the thickness (vertical distance between the lower edge and the top of the bridge) of the crossing bridge (1–3 m), the length of the crossing bridge (3–30 m), and the horizontal distance between Tx and the crossing bridge, respectively.
- $D_{\mathrm{Tx-Rx}}$ is the horizontal distance between Tx and Rx, which can be calculated based on the coordinates of Tx and Rx at the time.

B. Correlation of the Influence of Crossing Bridges

To completely describe the influence of crossing bridges, the correlation of the influence of bridges should be considered. For ease of analysis, the following concepts are defined.

- Related region: The related region of a bridge is defined as the region from the train entering the space under the bridge to the recovery of the LOS between Tx and Rx.
- Independent crossing bridge (ICB): When the related region of a crossing bridge has no overlap with the related region of other crossing bridges, this crossing bridge is described as an ICB. The concept "independent" here means that the influence of the crossing bridge has no correlation with the influence of other crossing bridges. When Rx is in the related region of the ICB, the received power is only influenced by the current bridge. As shown in Fig. 2(b), $Br1$, $Br2$, and $Br3$ are three crossing bridges. The light blue, red, and green areas are the related regions of $Br1$, $Br2$, and $Br3$, respectively. $D_{Br2-Br1}$ is the distance difference from the start point of the related region of $Br2$ to the end point of the related region of $Br1$; similarly, $D_{Br3-Br2}$ is the distance difference from the related region of $Br3$ to the related region of $Br2$. Both of these parameters can be easily calculated from the parameters in Fig. 2(a). As shown in Fig. 2(b), $D_{Br2-Br1} \geq 0$, $D_{Br3-Br2} \geq 0$, which means that there is no overlap between any two related regions; therefore, the influence of every crossing bridge is independent; all of these three bridges are ICBs.
- Crossing bridge group (CBG): When there is an overlap between the related regions of two or more crossing bridges, the crossing bridges are no longer independent but constitute a CBG. In the case shown in Fig. 2(c), $D_{Br2-Br1} < 0$, which implies that the end point of the related region of $Br1$ is further than the start point of the related region of $Br2$. Hence, in the overlapping parts (deep red area in the figure), the wave experiences not only the effect of $Br2$ but also the effect of $Br1$. Thus, the propagation of $Br2$ is different from the independent case. Similarly, in the case shown in Fig. 2(d), the influence of $Br3$ is not independent. All of the bridges in Fig. 2(e) are not independent; hence, the influence should be treated as a CBG. The different sizes and heights of the bridge schematics are used to show how the related regions appear when the dimensions of crossing bridges change.

C. Propagation Mechanism Zones of Crossing Bridges

Since propagation mechanisms differ when the Tx, crossing bridge (group), and Rx are in different positional relationships, the entire process should be divided into various zones. Fig. 3(a) and (b) shows the zone division for the ICB when the bridge is far and near the Tx, respectively. The following zones are defined.

- Zone A: When the Rx is in the narrow space under the crossing bridge but the LOS is still kept, the directed wave and multiple reflected waves from the track and the bridge are the main components of the received power.

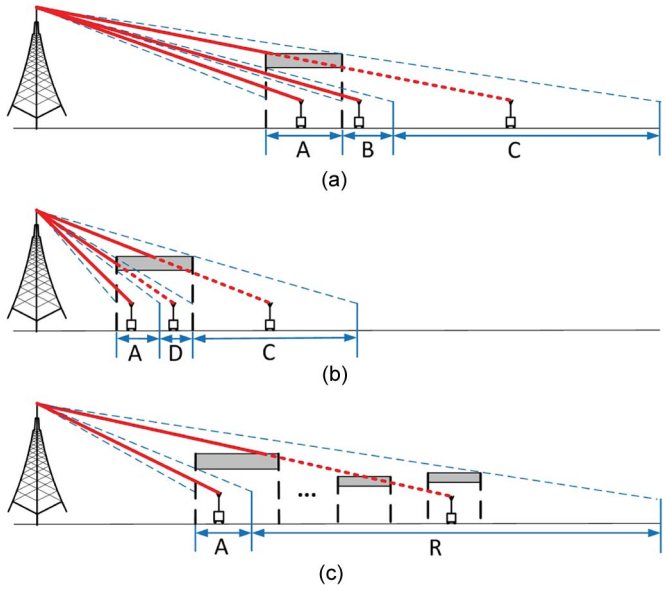

Fig. 3. (a) Propagation zone division for the ICB (the bridge is far from the Tx). (b) Propagation zone division situation for the ICB (the bridge is near the Tx). (c) Propagation zone division for the CBG.

- Zone B: When the Rx has passed the bridge but the LOS is still kept, the directed wave and reflected waves are the main components. There may be less "extra loss" and multipath effects than in Zone A, because the Rx is in a wider space than under the bridge.
- Zone C: When the Rx has passed but the LOS is blocked by the bridge, there is no directed wave from the Tx; hence, the reflected and diffracted waves dominate.
- Zone D: When the bridge is near the Tx, the LOS is blocked before the Rx passes the bridge. Hence, Zone D is the case when the Rx is under the bridge but under a non-LOS (NLOS) condition. No LOS exists, and the multipath propagation dominates. Fig. 3(b) shows the situation when the bridge is near. Zone A and Zone C are the same as in Fig. 3(a). The only difference is that Zone B is replaced by Zone D.

The situation in the CBG is shown in Fig. 3(c). Zone A is the same as in the ICB case. Since the influence of the bridges in the group is related to each other, it is very difficult to divide zones to cover every possibility. To facilitate the application, all the related regions are summarized into one zone, i.e., Zone R.

III. Measurement Campaign

A. Measurement System

The present GSM for railway (GSM-R) [25] network was utilized in the measurements. The detailed descriptions of the test system are as follows.

- Transmitter: Existing GSM-R base stations (BSs) are utilized as transmitters. The dual-polarization directional APX86-906515S-CT0 antennas, with 17-dBi gain, 65° horizontal, and 6.8° vertical beamwidths were mounted on towers and connected to the signal transmitter with a 100-m RFS 7/8 feeder cable (3.5-dB loss). The 3-D radiation pattern of transmitting antennas is shown in

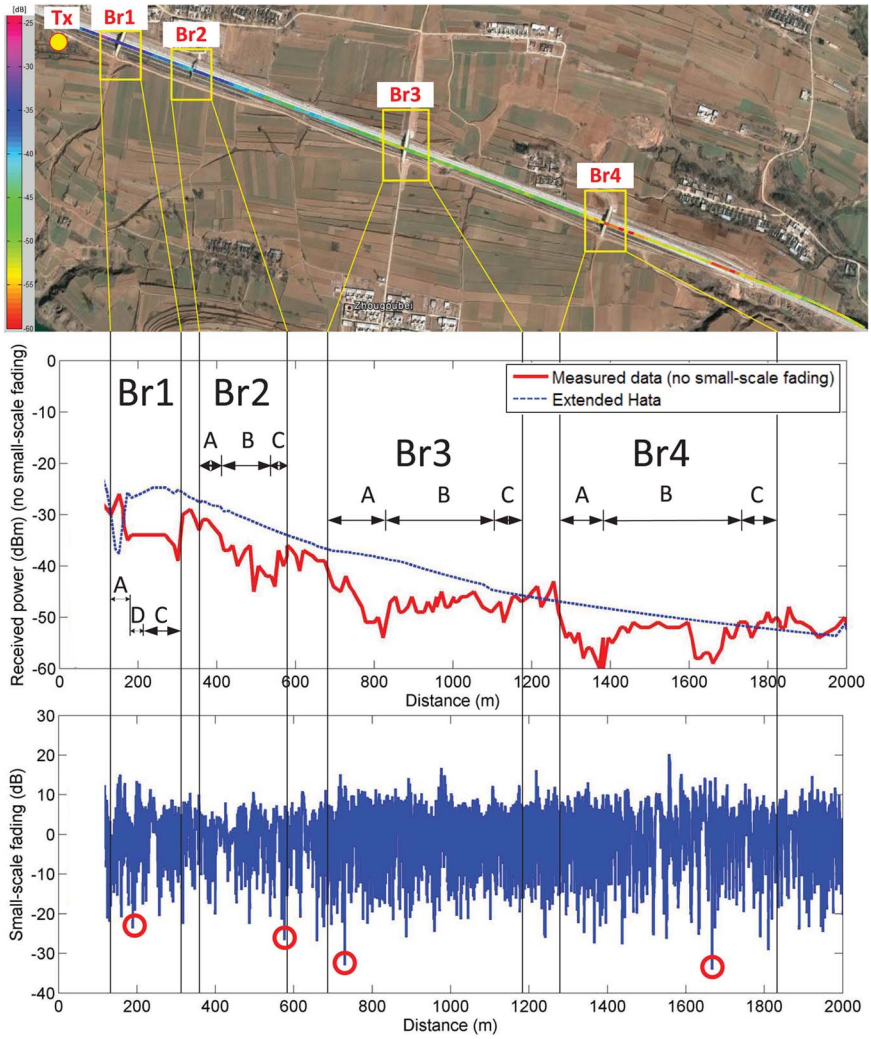

Fig. 4. Measured results in Case 1. Aerial view, received power without small-scale fading, and small-scale fading. (Red circles) Max. FVs in the related region of every bridge.

Fig. 1(c), which is interpolated by the horizontal and vertical patterns [26]. The broadcast control channel signal with carrier frequencies from 930.2 to 933.4 MHz with a bandwidth of 200 kHz was fed to the transmitting antenna. The transmitting power was 43 dBm. The power splitter with 3.01-dB loss was utilized to provide multichannel signals for the BS to cover the cells on both sides. Fig. 1(b) shows a photo of the BS antennas deployed 25–35 m higher than the track.

- Receiving antenna: The receiving antenna was an omnidirectional 900/2400-HBNT antenna, with 4-dBi gain, 80° vertical beamwidth, located in the middle part of the train, on the top of the carriage at a height of 30 cm above the roof, as shown in Fig. 1(d). The free-space 3-D radiation pattern of the receiving antenna is shown in Fig. 1(e). The receiving antenna and the receiver inside the train were connected by a 40-m 10D-FB feeder cable (3.3-dB loss).
- Other equipment: The train in the measurement was a representative CRH2 high-speed train that is 3.8 m high, 3.38 m wide, and 204.9 m long. A Willtek 8300 Griffin fast measurement receiver was utilized to collect and store measured data. The distance sensor was set on a wheel of the locomotive to record the wheel speed. Under the location-trigger mode and with the speed of the train up to 350 km/h, we have taken the samples at 53-cm (one measurement per 1.64 wavelength) intervals for large-scale fading and 10-cm (one measurement per 0.31 wavelength) intervals for small-scale fading. The measurement locations were resolved with a Global Positioning System receiver. The data display and statistical processing are conducted by a field strength measurement software on a portable computer. The lowest average signal-to-noise-ratio (SNR) measured at a particular location is approximately 30 dB. At most locations, the SNR is larger than 30 dB so that an accurate estimation of channel parameters is possible.

B. Measurement Environment

Extensive measurements were carried out along the Zhengzhou–Xi'an high-speed railway in China at 930 MHz during daytime in the fall of 2009. The dimensions, elevation,

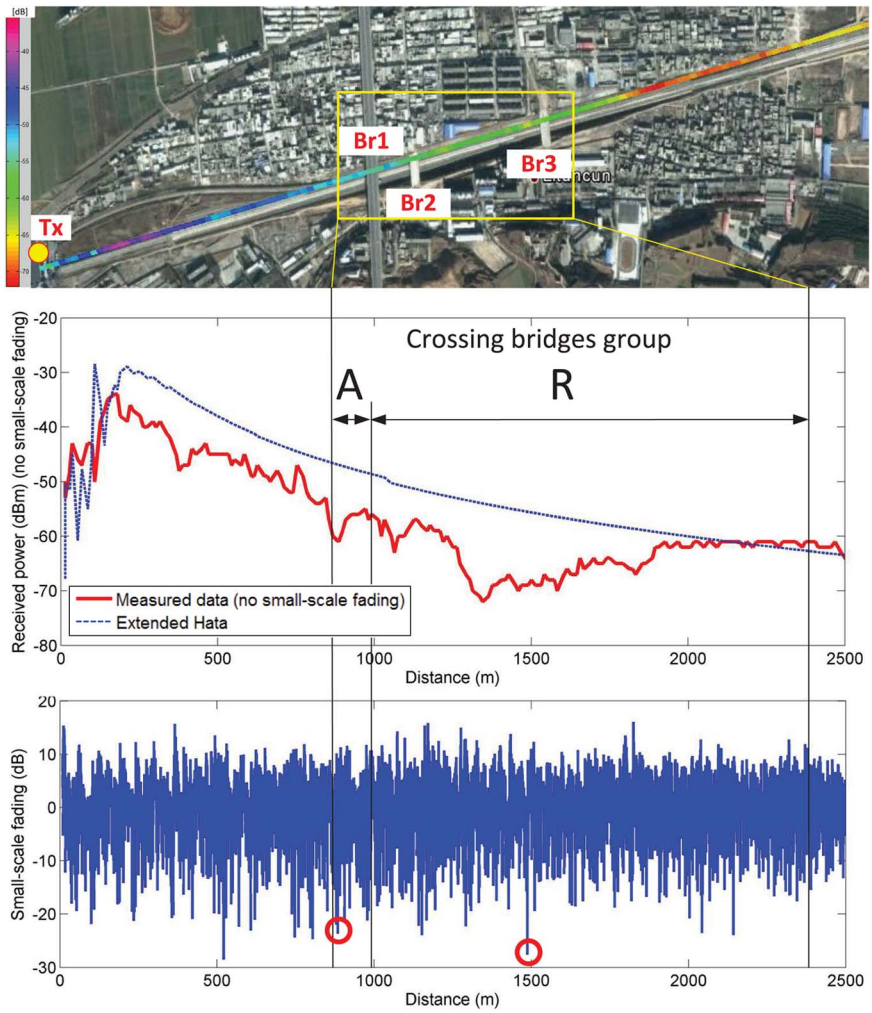

Fig. 5. Measured results in Case 2. Aerial view, received power without small-scale fading, and small-scale fading. (Red circles) Max. FVs in Zone A and Zone R of the CBG.

and geographic coordinates of the track and transmitters are supported by China Railway Survey and Design Group Co. Ltd. The dimensions and heights (relative to the track) of crossing bridges were manually measured by a laser distance meter. The resolution of terrain raster data is originally from Shutter Radar Topography Mission (SRTM) [27] with a resolution of 90 m and finally regridded up to 10 m by interpolation.

Based on the given analysis, two typical scenarios were selected for measurements. Fig. 4 gives the aerial view of Case 1. The blue lines indicate the rail tracks. In this case, the distances between the related regions of every two adjacent bridges ($D_{Br2-Br1}$, $D_{Br3-Br2}$, and $D_{Br4-Br3}$) are positive. Hence, the influence of each bridge is independent, and therefore, this type of bridge can be defined as an ICB. Case 2 is shown in Fig. 5, in which crossing bridges are concentrated. Since both $D_{Br2-Br1}$ and $D_{Br3-Br2}$ are negative, which means the influence of each bridge correlates, Case 2 effectively reflects the influence of a CBG. For each case, the multiple measurements were taken by the moving train to reproduce as closely as possible "real" operation. Parameters of scenarios are given in Table I, where θ and ϕ are the elevation angle (0° upward) and the azimuth angle (0° norward, clockwise rotation) of transmitting antennas, respectively.

IV. Measurement Results and Analysis

A. Elimination of the Influence of Antenna Pattern

As shown in Fig. 1(c) and (e), the free-space 3-D radiation patterns of the transmitting antenna and the receiving antenna are obtained by the interpolation (with 1° resolution) of their own horizontal and vertical patterns. Then, by knowing the geometrical relation of Tx and Rx and the setup of elevation and azimuth angles of transmitting antennas (given in Table I), the antenna gain at all the angles of arrival or departure is fully described. Thus, the influence of (free space) antenna patterns can be effectively eliminated when we analyze the measured results.

B. Data Analysis

Figs. 4 and 5 show the aerial view, received signal power without small-scale fading, and small-scale fading in the measured results of Case 1 and Case 2, respectively. Here, small-scale fading is separated from the received power by averaging samples at intervals of 13 m (40 wavelengths) [28]. Except for crossing bridges, there are no obstructions such as tall trees or buildings in the propagation path in the measurement scenarios.

TABLE I
PARAMETERS OF MEASUREMENTS

Case 1:	Independent Crossing Bridge (ICB)		
H_{Tx} (m)	Polarization	θ°	ϕ°
33	Dual +/-45°	4	110
Frequency:	930.2 MHz	Height of Rx:	4.1 m
No. Br	H_{Br} (m)	L_{Br} (m)	T_{Br} (m)
Br1	18.87	8.52	2.05
Br2	17.11	3.17	1.44
Br3	12.36	9.57	1.95
Br4	12.24	8.64	2.37
$D_{Br2-Br1}$:		31.62 m	
$D_{Br3-Br2}$:		113.94 m	
$D_{Br4-Br3}$:		145.47 m	
Case 2:	Crossing Bridges Group (CBG)		
H_{Tx} (m)	Polarization	θ°	ϕ°
32	Dual +/-45°	4	73
Frequency:	932.4 MHz	Height of Rx:	4.1 m
No. Br	H_{Br} (m)	L_{Br} (m)	T_{Br} (m)
Br1	14.81	28.88	2.84
Br2	15.24	21.92	2.32
Br3	12.27	21.54	2.17
$D_{Br2-Br1}$:		-468.44 m	
$D_{Br3-Br2}$:		-291.23 m	

Thus, to better observe the extra loss resulting from the crossing bridges, the open-area environment in the extended Hata model [29] can be utilized to be a reference that shows the situation when no crossing bridge exists. The choice of the Hata family of models for the comparison with measurements is as follows.

- In the measurement scenarios, apart from crossing bridges, there are no obstructions and few scatterers along the railway between Tx and Rx. This character is close to the description of the open-area environment in the Hata family of models.
- The Hata family of models has already been widely used in the network planning and interference analysis of GSM and GSM-R.
- The open and suburban environments of the Hata family of models have been justified to be proper for the railway environment by comparisons to extensive measurements in [30] and [31]. In [32], the Hata family of models has been considered as a path loss model for train-to-train communication as well.

It is noteworthy that the Rx antenna pattern shown in Fig. 1(e) is the free-space pattern, not the actual pattern measured by the antenna in combination with the carriage. Nevertheless, as shown in Fig. 4, the received power predicted by the extended Hata model combined with the free-space antenna pattern has good agreement with the measured result in the places where no crossing bridge exists. This means that the extended Hata model combined with the free-space antenna pattern supports a good reference in this case, and therefore, the significant affection from the antenna pattern distortion to the extracted extra loss is not expected.

Based on extensive experimental results, all the propagation characteristics, including extra propagation loss with respect to the extended Hata model, shadow fading, small-scale fading, and fading depth (FD), have been derived and summarized in Table II.

1) Extended Hata Model: The Hata model was originally developed for NLOS paths in urban environments. In [29] and [33], the model was extended so that the extended Hata model can predict outdoor propagation loss in the 30–3000-MHz band for various environments. The extended Hata model is a piecewise function of d in kilometers, which denotes the distance between Tx and Rx. When $d < 0.04$, the median path loss is given by

$$L = 32.4 + 20\log(f) + 10\log\left[d^2 + \frac{(H_b - H_m)^2}{10^6}\right] \quad (1)$$

where L denotes the path loss (in decibels) and f is the frequency (in megahertz). H_b denotes the maximum of the heights of Tx and Rx (in meters), whereas H_m denotes the minimum of the heights of Tx and Rx (in meters).

When $0.04 \le d < 0.1$, the path loss is expressed by

$$L = L(0.04) + \frac{[\log(d) - \log(0.04)]}{[\log(0.1) - \log(0.04)]} \cdot [L(0.1) - L(0.04)]\,. \quad (2)$$

When $d \ge 0.1$, the path loss of the open area in the extended Hata model is given by

$$L = L(\text{urban}) - 4.78 \cdot \{\log[\min\{\max\{150; f\}; 2000\}]\}^2 + 18.33 \cdot \log[\min\{\max\{150; f\}; 2000\}] - 40.94 \quad (3)$$

where $L(\text{urban})$ denotes the path loss in the urban environment. When the frequency is between 150 and 1500 MHz, the value of $L(\text{urban})$ is given by

$$L(\text{urban}) = 69.6 + 26.2\log(f) - 13.82\log(\max\{30, H_b\}) + [44.9 - 6.55\log(\max\{30, H_b\})] \times (\log(d))^\alpha - a(H_m) - b(H_b) \quad (4)$$

where

$$a(H_m) = (1.1\log(f) - 0.7) \cdot \min\{10; H_m\} - (1.56\log(f) - 0.8) + \max\{0; 20\log(H_m/10)\} \quad (5)$$

$$b(H_b) = \min\{0; 20\log(H_b/30)\} \quad (6)$$

$$\alpha = 1\,(d \le 20)\,. \quad (7)$$

2) Extra Propagation Loss Compared to the Extended Hata Model: As shown in Figs. 4 and 5, extra propagation loss (compared to the extended Hata model) owing to the crossing bridges is clearly reflected. As shown in Fig. 4, all the propagation zones of each bridge are well distinguished and in good agreement with the given theoretical analysis. Fig. 5 shows the situation in Case 2. Since Zone R reflects the overall effect of the three related crossing bridges, its attenuation profile differs from any independent zone. The maximum attenuation of up to 24.00 dB has been observed in Zone R. This value is much larger than the estimated value of 5 dB in [24], and this means that the only known insight into the influence of crossing bridges is overly optimistic for the cases studied here.

TABLE II
RESULTS OF MEASUREMENTS

Case	Independent Crossing Bridge (ICB)				Crossing Bridges Group (CBG)	
Zone	A	B	C	D	A	R
Extra Propagation Loss compared to the Extended Hata Model						
Max	15.51 dB	15.27 dB	10.10 dB	13.83 dB	20.06 dB	24.00 dB
Min	-2.39 dB	1.01 dB	-3.23 dB	4.39 dB	3.73 dB	6.88 dB
Mean	6.55 dB	5.96 dB	6.25 dB	9.11 dB	9.66 dB	14.18 dB
Median	8.13 dB	5.68 dB	6.44 dB	9.48 dB	9.12 dB	13.90 dB
Std	6.98 dB	3.22 dB	3.68 dB	6.68 dB	4.02 dB	3.11 dB
Shadow Fading						
Distrib.	Normal in dB	Normal in dB	Normal in dB	Normal in dB	Normal in dB	Normal in dB
Std	4.73 dB	2.40 dB	2.46 dB	3.55 dB	1.98 dB	1.88 dB
Small-Scale Fading						
Distrib.	Ricean	Ricean	Ricean	Ricean	Ricean	Nakagami
Parameter	K = -3.79 dB	K = 0.10 dB	K = -11.07 dB	K = -12.89 dB	K = -3.32 dB	m = 1.31
Fading Depth						
Max. FV	-37.06	-31.76	-18.34	-36.23	-43.11	-43.78
1%	-26.33	-17.83	-14.17	-12.95	-20.03	-25.59
50%	1.63	1.07	1.91	2.09	1.87	1.77
FD	27.96	18.91	16.09	14.88	21.89	27.36
Max. FD	38.69	32.83	20.25	19.80	44.98	45.55

3) Shadow Fading: Shadow fading is extracted from the path loss based on the following expression:

$$L(d) = \overline{L}(d) + X_\sigma = \overline{L}(d_0) + 10n \lg\left(\frac{d}{d_0}\right) + X_\sigma \qquad (8)$$

where d_0 denotes the referenced distance, n denotes the path loss index, X_σ denotes shadow fading, and $\overline{L}(d)$ and $\overline{L}(d_0)$ denote the media path loss and path loss at d_0, respectively. Then, the given equation can be used to calculate the shadow fading values by a simple minus. $\overline{L}(d_0)$ and index n can be received by the least squares criterion.

By passing Kolmogorov–Smirnov, Anderson–Darling, and Chi-Squared tests in Easy Fit [34], shadow fading in every zone is well fitted by the lognormal distribution, which is the most common model that is empirically confirmed for fitting shadow fading [35]. The shadow fading standard deviations (Stds) (σ) in every zone based on the averaging of repeated measurements are listed in Table II. It can be seen that the values of σ change from 1.88 to 4.73 dB, which are larger than the corresponding values (1.56–2.84 dB) in the viaduct scenario in [3] where no crossing bridge exists.

4) Small-Scale Fading: A number of different distributions have been proposed for small-scale fading in high-speed railway environments [7], [18], [36], [37], and various justifications have been given for them. The most prominent among them are Ricean, Rayleigh, and Nakagami distributions. To keep good comparability to the other scenarios in a high-speed railway, we consider these three distributions as appropriate functional fits to the measured fading distributions. Thus, the distribution estimation for all nonoverlapping 10-m windows is conducted. This window length includes a sufficient number of samples (100 samples for a 10-cm sampling interval) to allow a reasonable testing of the distribution fit and also provides an efficient tradeoff between the accuracy and complexity of data processing. Ricean, Rayleigh, and Nakagami distributions are utilized for the fitting. All of these three distributions have passed Kolmogorov–Smirnov, Anderson–Darling, and Chi-Squared tests in Easy Fit [34]. Fig. 6 shows the empirical cumulative distribution function (cdf) and theoretical model fits of the envelope levels in each propagation zone based on multiple measurements.

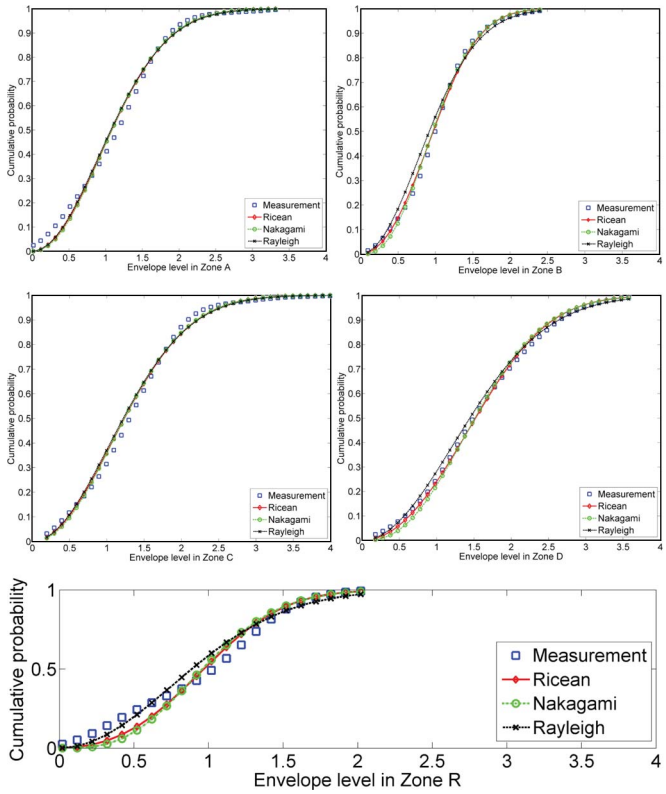

Fig. 6. Empirical cdfs of the small-scale fading amplitudes and their theoretical model fitting in Zone A, Zone B, Zone C, Zone D, and Zone R.

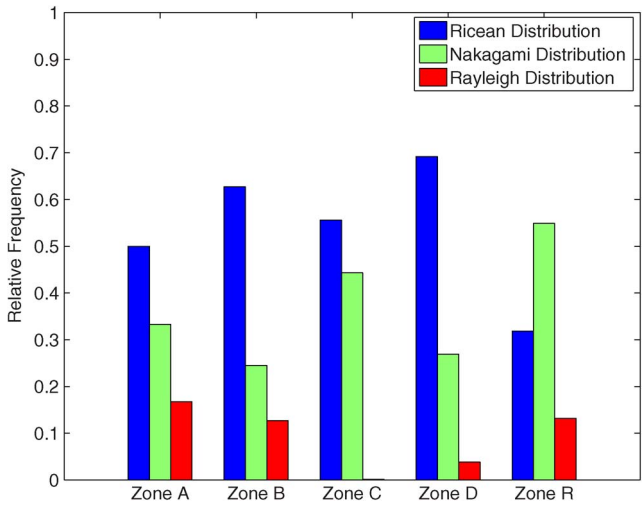

Fig. 7. Relative frequency of AIC selecting each of the candidate distributions as best fit in all the propagation zones based on multiple measurements.

To make a comparison among these three distributions and conclude which one can best fit the small-scale fading in the regions related to crossing bridges, Akaike's information criterion (AIC) is employed. AIC is an asymptotically (in sample size) unbiased estimator of the relative expected Kullback–Leibler (KL) distance between the operating model and the candidate distributions and, thus, allows the selection of the model with the smallest KL distance to the measurements [38]. This measure of the relative goodness-of-fit of a statistical model has been widely used in the selection of distribution fit [38]–[40]. The AIC for the jth candidate distribution that has a probability density function (pdf) $g_{\widehat{\theta}_j}$ is given by

$$AIC_j = -2\sum_{n=1}^{N} \log_e \left[g_{\widehat{\theta}_j}(x_n) \right] + 2U \tag{9}$$

where g denotes the pdf of the candidate distribution, and $g_{\widehat{\theta}_j}$ denotes the maximum-likelihood estimate of the distribution parameter vector θ_j obtained from the measurements. U denotes the dimension of vector $\widehat{\theta}_j$ (Rayleigh distribution: U = 1; Ricean and Nakagami distributions: U = 2). N denotes the size of sample set $X = x_1, \ldots, x_N$. The model with the lowest AIC provides the best fit.

Fig. 7 shows the relative frequency of AIC selecting each of the candidate distributions as best fit in all the propagation zones based on multiple measurements. The corresponding findings are as follows.

- The Ricean distribution provides the best fit for the time-varying envelopes in Zone A, Zone B, Zone C, and Zone D. As the indicator of the proportion of the dominant component in the signal power, the Ricean K-factor is estimated by using the time-saving moment-based method in [42] and [43], which can be expressed as

$$K = \frac{\sqrt{1 - \frac{\mathrm{Var}[r^2]}{(E[r^2])^2}}}{1 - \sqrt{1 - \frac{\mathrm{Var}[r^2]}{(E[r^2])^2}}} \tag{10}$$

where r denotes the small-scale fading amplitude, $E[\bullet]$ denotes the expected value of $[\bullet]$, and Var$[\bullet]$ denotes the variance of $[\bullet]$. In this paper, the K-factor is estimated for all nonoverlapping 10-m windows in Zone A, Zone B, Zone C, and Zone D. The mean value of the K-factor in Zone A and Zone B varies from -3.79 to 0.10 dB, which is much smaller than the mean value of 3.79 dB of the K-factor in the viaduct scenario [4], even smaller than the value of 1.88 dB in the cuts scenario [5]. This finding indicates that the reflection and scattering from the bridge and the track continue to be present to a large extent when the train is under the crossing bridge or has passed the bridge but is still in the related region.
- Note that although the AIC test rarely gives the Rayleigh distribution as the optimum distribution, the mean values of the K-factor in Zone C and Zone D are from -11.07 to -12.89 dB, which is small enough to allow description of the fading as Rayleigh. This indicates that the blocking effect of the crossing bridge leads to a very weak LOS in Zone C and Zone D, which means that the channel in these two zones can be treated as the NLOS condition.
- The best fitting result in Zone R is the Nakagami distribution. Parameter m is 1.31, estimated by using the moment method derived in [41], which implies that the fluctuations in the signal strength are smaller than Rayleigh fading but stronger than Ricean fading. This matches well the structural features of the CBG. The related bridges generate multiply scattered waves and different clusters of reflected waves. In addition, this is the typical environment of Nakagami fading.

5) FD: As an important parameter of fading behavior, FD in every zone has been investigated. The FD is obtained from the difference in signal levels between the 50% and 1% values. The maximum FD (Max. FD) is derived from the difference in signal levels between the 50% and maximum fading values (Max. FVs) [44]. All of the results are summarized in Table II. It is shown that in the crossing bridge related regions, the FD is between 14.88 and 27.96 dB, whereas the Max. FD is between 19.80 and 45.55 dB. Both parameters are obviously larger than the corresponding values in the viaduct scenario in [2] due to the effect of crossing bridges.

V. Modeling for the Extra Propagation Loss

The crossing bridge is a kind of obstacle, and therefore, the modeling for the extra propagation loss owing to the bridge is of great interest. As shown in Figs. 4 and 5, the extended Hata model successively predicts the path loss in the cuts scenario when no crossing bridge exists but fails to reflect the extra loss resulting from the bridges. To support an effective way to predict the propagation in the related regions of crossing bridges, two empirical models for the extra loss are presented.

A. Modeling for the Extra Loss of the ICB (ICB Model)

The difficulty in modeling is the structure of the crossing bridge. A basic idea is to try to use some multiedge diffraction models (such as the Deygout model [45], the Epstein–Peterson

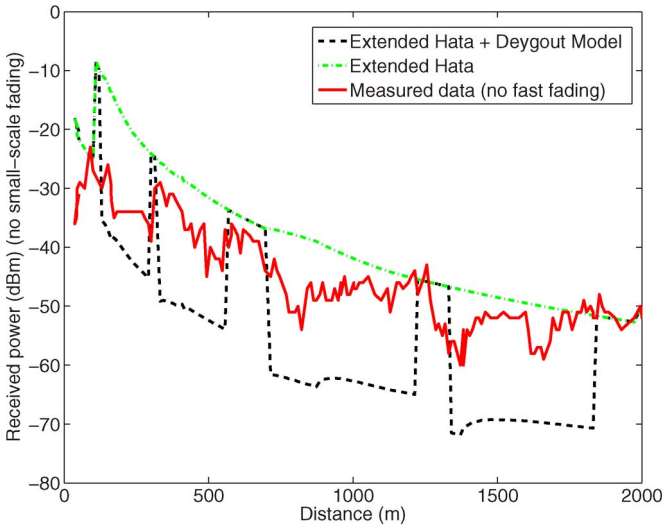

Fig. 8. Comparison on the received power (no small-scale fading) between the predicted result of the Deygout model and the measured result in Case 1.

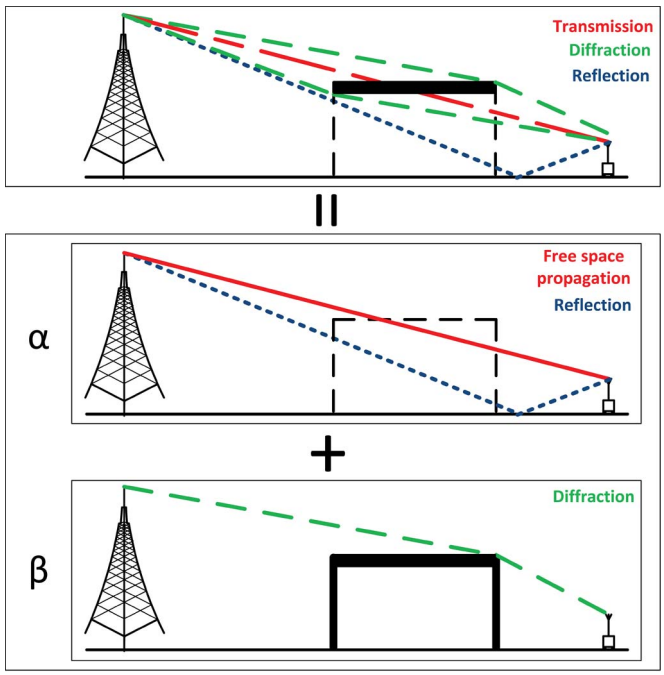

Fig. 9. Sketch of the modeling of the ICB (ICB model). The final propagation can be treated as the combination of the subcase when no bridge exists and the subcase when the bridge is a solid obstacle with weight coefficients α and β.

model [46], etc.) to modify the Hata model, which has been widely used in commercial prediction tools and academic research (e.g., "Hata + Epstein–Peterson" in [47]–[49] and "Hata + Deygout" in [47], [48], [50], and [51]). Fig. 8 shows a comparison on the received power between the predicted result of the Deygout model [45] (the black dashed line) and the measured result (the red line) in Case 1. Here, the Deygout model is implemented by treating the crossing bridge as a solid obstacle, which is the second subcase shown in Fig. 9. It is shown in Fig. 8 that the measured power is stronger than the predicted result of the Deygout model. This implies that the crossing bridge is not a solid obstacle, certain free space exists under the bridge so that the LOS can be kept even when the receiver is under or passes the bridge. Hence, the propagation loss can be considerably overestimated by directly using the existing diffraction models that are established for the solid obstacles, such as buildings, mountains, etc. However, we can still get the basic idea of modeling in Fig. 8 with Fig. 4. The received power is higher than in the case when the bridge is a solid obstacle and lower than in the case when no obstacle exists. This indicates that the extra loss can be modeled by the combination of the two cases (solid obstacle and no obstacle). In fact, this idea has been successively used for the multiedge diffraction modeling. The most frequently used models are the Epstein–Peterson model [46] and the Deygout model. Both of them calculate the total diffraction loss of the multiedge by combining more than one application of the single knife-edge model [52].

As shown in Fig. 9, transmission, diffraction, and reflection are the main propagation mechanisms when the Rx is behind the crossing bridge. The first subcase is without any obstruction related to the bridge; the received signal power consists of the free-space propagation and reflection. The second subcase treats the bridge as a solid obstacle; the received signal is affected only by diffraction. Similar to the Epstein–Peterson model and the Deygout model, the final result can be treated as the combination of the two subcases with weight coefficients α and β. According to the concrete mechanisms that have been analyzed in Section III-A, the values of α and β in every propagation zone could be different. Thus, least squares (LS) fitting is required to be utilized for every zone to get the regression coefficients in every zone. The formula of the extra loss of ICB (ICB model) can be presented as

$$L_{\rm br} = \alpha_i \cdot L_{dif1} + \beta_i \cdot L_{dif2}, \quad \alpha_i + \beta_i = 1,\ i = A, B, C, D \tag{11}$$

where $L_{\rm br}$ denotes the extra propagation loss of the ICB, and $L_{\rm dif1}$ and $L_{\rm dif2}$ denote the diffraction loss in the first subcase and the second subcase, respectively. Both $L_{\rm dif1}$ and $L_{\rm dif2}$ can be calculated by the aforementioned classical multiedge diffraction models. $L_{\rm br}$, $L_{\rm dif1}$, and $L_{\rm dif2}$ are measured in decibels. α_i and β_i denote the regression weight coefficients in every zone.

1) Implementation of Deygout Model: In this paper, the Deygout model is chosen because of its good performance (e.g., in [53]). By determining the main obstacle (HK1) with the Fresnel parameter υ_1 and effective height H_1, the subobstacle (HK2) between the Tx and the HK1 with υ_2 and effective height H_2, and the subobstacle (HK3) between the HK1 and the Rx with υ_3 and effective height H_3, the final diffraction loss of the Deygout model can be obtained by linearly combining the corresponding three diffraction losses [55]

$$\mathrm{L_{dif}} = L_1(\upsilon_1) + L_1(\upsilon_2) + L_1(\upsilon_3) \quad \text{in dB} \tag{12}$$

where

$$L_i = \gamma \cdot 20 \lg(|A_i|) \tag{13}$$

and where γ is the knife-edge correction factor, which is 0.35 in the implementation of the Deygout model in this paper, i.e.,

$$A_i = \frac{1}{\sqrt{\pi}} e^{v_i^2} \int_{v_i}^{\infty} e^{-x^2} dx, \qquad i = 1 \ldots 3 \tag{14}$$

$$v_1 = \left(\frac{H_1 - H_{\mathrm{Tx}}}{d_1 + d_2} + \frac{H_1 - H_{\mathrm{Rx}}}{d_3 + d_4} \right) \cdot \sqrt{\frac{ik(d_1 + d_2)(d_3 + d_4)}{2(d_1 + d_2 + d_3 + d_4)}} \tag{15}$$

$$v_2 = \left(\frac{H_2 - H_{\mathrm{Tx}}}{d_1} + \frac{H_2 - H_1}{d_2} \right) \cdot \sqrt{\frac{ikd_1 d_2}{2(d_1 + d_2)}} \tag{16}$$

$$v_3 = \left(\frac{H_3 - H_1}{d_3} + \frac{H_3 - H_{\mathrm{Rx}}}{d_4} \right) \cdot \sqrt{\frac{ikd_3 d_4}{2(d_3 + d_4)}} \tag{17}$$

where d_1, d_2, d_3, and d_4 are the distance between Tx and HK2, between HK2 and HK1, between HK1 and HK3, and between HK3 and Rx, respectively. k is the wavenumber in the vacuum. Since the Deygout method always overestimates the diffraction loss, particularly when two obstacles are close to each other, there are two options to offset the overestimation.

- Use the approximation presented in [54] to compute the multiple diffraction losses. The analytical basis for the method of Deygout, taking into account the rigorous spectral diffraction theory outside the transition regions surrounding the shadow boundaries, is used to explain the suggested modification in [54].
- Use the following correction factor from Causebrook [55]:

$$L_B = L_2(v_1) + L_1(v_2) + L_3(v_3) - C_1 - C_2 \tag{18}$$

$$C_1 = (6 - L_2(v_1) + L_1(v_2)) \cos \alpha_1 \tag{19}$$

$$C_2 = (6 - L_2(v_1) + L_3(v_3)) \cos \alpha_2 \tag{20}$$

$$\cos \alpha_1 = \sqrt{\frac{d_1(d_3 + d_4)}{(d_1 + d_2)(d_2 + d_3 + d_4)}} \tag{21}$$

$$\cos \alpha_2 = \sqrt{\frac{d_4(d_3 + d_4)}{(d_1 + d_2)(d_1 + d_2 + d_3)}}. \tag{22}$$

In this paper, the correction factor from Causebrook is implemented.

2) Estimation of Weight Coefficients: Most information determining the extra propagation loss has been considered by the propagation mechanism zone division (in Section II-C) and the implementation of the Deygout model, such as the frequency of the wave, the dimension and shape of the crossing bridge, positional relationships among Tx, crossing bridge, and Rx, etc. However, some factors such as frequency and polarization of the wave and material of the obstacle lead to different values of weight coefficients α_i and β_i in different propagation zones. Hence, the weight coefficients should be estimated from some small-scale measurements when the model is established. In this paper, the coefficients estimated by four crossing bridges can be successfully used for the other 15 bridges with different dimensions along a high-speed railway without further measurements. This gives us reason to believe that the presented model can effectively predict the extra loss owing to the crossing bridges at the 930-MHz frequency band.

TABLE III
ME, STD, AND RMSE BETWEEN MEASUREMENT AND PREDICTION WITH WEIGHT COEFFICIENTS REGRESSED IN EVERY ZONE OF Br1, Br2, Br3, AND Br4 IN CASE 1

Case 1	Br1	Br2	Br3	Br4
α_A	0.56	0.50	0.55	0.43
α_B	-	0.68	0.73	0.71
α_C	0.50	0.52	0.64	0.54
α_D	0.00	-	-	-
ME (dB)	0.4	0.1	0.8	0.8
Std (dB)	5.4	2.5	2.6	3.2
RMSE (dB)	5.4	2.5	2.7	3.3

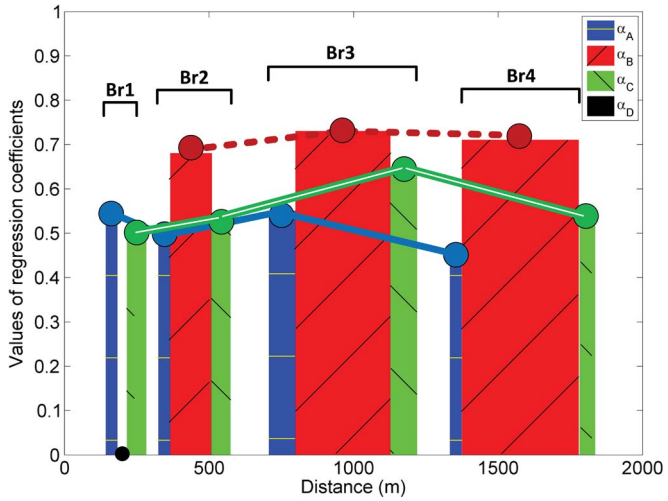

Fig. 10. Values of regression coefficients along the distance between Tx and Rx in Case 1.

The values of the weight coefficients are estimated by using LS fitting in every zone of every crossing bridge in Case 1 based on repeated measurements. The mean error (ME), Std, and root mean square error (RMSE) between the measurements and the results of the model with estimated coefficients are summarized in Table III. The reason why α_D is only estimated in $Br1$ is because Zone D only exists when the crossing bridge is very near the Tx. When the Rx is not so close to the Tx, Zone D is replaced by Zone B.

Fig. 10 shows the values of regression coefficients along the distance between Tx and Rx. It can be found that the coefficients slightly change along with the distance. However, the values of each coefficient stabilize in a small change interval (0–0.14). Considering the uncertainty in the measurements and the inaccuracy of the raster data from SRTM, we decide not to connect these values to the distance but to use the mean value of each coefficient to represent the typical situation at 930 MHz in the distance range (0–2000 m), which is the typical size of a GSM-R cell. These mean values of parameters are listed in Table IV. α_B is the largest, which means that the extra loss is the smallest. In addition, this meets the character of Zone B, i.e., with LOS and in the wide space. The conditions of Zone A and Zone C are opposite, i.e., Zone A is with LOS but in the narrow space under the bridge, whereas Zone C is in the wide

TABLE IV
PARAMETERS OF THE PRESENTED MODEL FOR THE ICB (ICB MODEL)

Zone	Zone A	Zone B	Zone C	Zone D
α	0.51	0.68	0.55	0
β	0.49	0.32	0.45	1

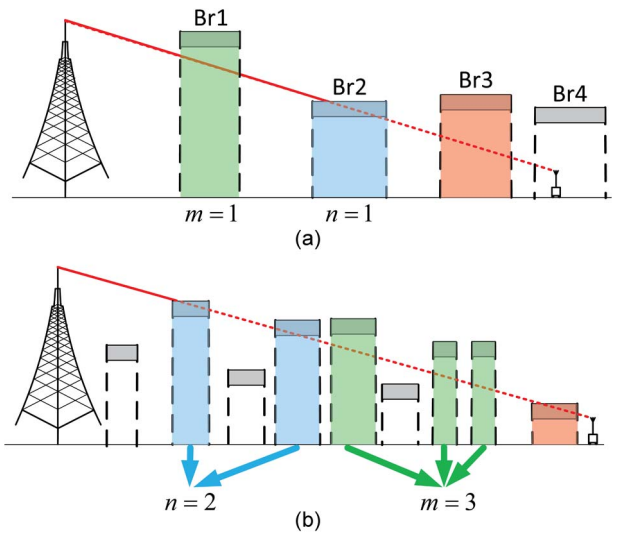

Fig. 11. (a) Sketch of a simple case of the CBG. The Rx is in Zone B of the original bridge Br3; Br1 and Br2 are the additional bridges. Before arriving at the original bridge Br3, the LOS passes through Br1 and is blocked by Br2. (b) Sketch of a general case of the CBG. Before arriving at the original bridge, the LOS passes through m additional bridges and is blocked by n additional bridges.

space but with NLOS. Thus, the finding that α_A is smaller than α_C implies that in the related regions of crossing bridges, the dimension of the space is more critical than the condition of LOS. With NLOS and in the narrow space, this character of Zone D leads to a 0 value of α_D, which indicates that the extra loss in Zone D can be treated as the result of a solid obstacle. The values of the regression coefficients in the model confirm the theoretical analysis in Section II-C.

B. Modeling for the Extra Loss of CBG (CBG Model)

The modeling for the extra loss of CBG (CBG model) is more complex than in the case of the ICB. Based on the analysis in Section II, the regions of a CBG are always the overlapping parts of the related regions of different crossing bridges. This means that before reaching the last bridge before the Rx (defined as the original bridge), the propagation wave has already experienced a certain influence of the additional bridges.

Taking the LOS for instance, the most common influence of the additional bridge occurs when the LOS is blocked by the bridge or when the LOS passes through the narrow space under the bridge. Fig. 11(a) shows a typical CBG. The LOS between the Tx and the Rx is blocked by Br2 and passes through Br1 and Br3. If the additional Br1 and Br2 do not exist, it is a typical situation that the Rx is in Zone B of the original bridge Br3. Note that the Rx is not in Zone A of Br4, because the last bridge that the LOS passes through or penetrates is Br3, and the LOS in Zone A should be directly transmitted from the Tx; hence, the Rx should be judged to be in Zone B of Br3. Since Br1 and Br2 influence the propagation in turn, by using the additional principal, the part $\beta_i \cdot L_{\mathrm{dif2}}$ in (1) representing the loss owing to the influence of one bridge can be added for expressing the loss resulting from additional bridges. Hence, the final extra loss in the case in Fig. 11(a) can be given by

$$L_g = \frac{\alpha_B \cdot L_{\mathrm{dif1}} + \beta_B \cdot L_{\mathrm{dif2}} + 1 \cdot \beta_B \cdot L_{\mathrm{dif2}} + 1 \cdot \beta_C \cdot L_{\mathrm{dif2}}}{\alpha_B + \beta_B + 1 \cdot \beta_B + 1 \cdot \beta_C} \tag{23}$$

where L_g denotes the extra loss of the CBG in decibels. α_B (in $\alpha_B \cdot L_{\mathrm{dif1}}$) and β_B (in $\beta_B \cdot L_{\mathrm{dif2}}$) denote the weight coefficients of Zone B because the Rx is in Zone B of Br3 (the original bridge). The two added parts $1 \cdot \beta_B \cdot L_{\mathrm{dif2}}$ and $1 \cdot \beta_C \cdot L_{\mathrm{dif2}}$ indicate the loss from the additional bridges Br1 and Br2, respectively. The coefficient of the effect of Br1 is β_B because the LOS passes through Br1; hence, the Rx can be treated to be in Zone B of Br1. Similarly, the Rx can be regarded to be in Zone C of Br2; hence, the coefficient of the extra influence of Br2 is β_C. The denominator normalizes all the coefficients.

Fig. 11(b) shows a more general case of the CBG. n is the number of additional bridges (blue) blocking the LOS, and m is the number of the additional bridges (green) that the LOS passes through. The red bridge denotes the original bridge that is the last bridge influencing the signal. The general type of the CBG model can be described as

$$L_g = \frac{\alpha_i \cdot L_{\mathrm{dif1}} + \beta_i \cdot L_{\mathrm{dif2}} + m \cdot \beta_B \cdot L_{\mathrm{dif2}} + n \cdot \beta_C \cdot L_{\mathrm{dif2}}}{\alpha_i + \beta_i + m \cdot \beta_B + n \cdot \beta_C} \quad i = A, B, C, D. \tag{24}$$

C. Validation for ICB Model and CBG Model

The accuracy of the proposed ICB model and CBG model is evaluated by the other 15 crossing bridges in three validation scenarios of the Zhengzhou–Xi'an high-speed railway:

- validation scenario 1: a 7-km duration full of ten crossing bridges (three bridges are independent; seven bridges constitute two CBGs) with different heights, widths, and thicknesses;
- validation scenario 2: a 1500-m duration with one CBG including two bridges;
- validation scenario 3: Case 2 in the measurement but not used to regress the coefficients; 2300-m duration with three crossing bridges constituting one bridges group.

The test system for validation is a standard GSM-R system that is the same as the test system used in the measurement campaign in Section II-A. All details of the parameters in the validation scenarios are summarized in Table V.

Fig. 12 shows the aerial view of validation scenario 1 and comparisons on the path loss between the measurements and different models. The extended Hata model (green dashed line) performs well in places that are not the related regions of crossing bridges; however, it fails to reflect the extra loss of crossing bridges. Hence, a deviation of up to 19.48 dB occurs, and this leads to a predicted result that is too optimistic. Contrarily, the

TABLE V
PARAMETERS OF VALIDATION SCENARIOS

Validation Scenario 1			
H_{Tx} (m)	Polarization	θ°	ϕ°
34	Dual +/-45°	3	109
Frequency:	932.4 MHz	Height of Rx:	4.1 m
No. Br	H_{Br} (m)	L_{Br} (m)	T_{Br} (m)
Br1	15.15	9.98	1.80
Br2	17.93	13.07	2.20
Br3	14.04	13.62	2.10
Br4	16.00	4.25	1.10
Br5	17.11	16.07	2.40
Br6	10.50	19.10	2.50
Br7	11.95	8.58	2.00
Br8	11.92	3.38	1.00
Br9	11.00	9.69	2.00
Br10	8.85	8.67	2.00
Validation Scenario 2			
H_{Tx} (m)	Polarization	θ°	ϕ°
28	Dual +/-45°	5	284
Frequency:	930.4 MHz	Height of Rx:	4.1 m
No. Br	H_{Br} (m)	L_{Br} (m)	T_{Br} (m)
Br11	14.29	10.90	2.40
Br12	12.05	11.69	2.60
Validation Scenario 3 = Measurement Case 2			
Br13 (Validation Scenario 3) = Br1 (Measurement Case 2)			
Br14 (Validation Scenario 3) = Br2 (Measurement Case 2)			
Br15 (Validation Scenario 3) = Br3 (Measurement Case 2)			

direct employment of the Deygout model (gray dashed line) considerably overestimates the extra loss. This implies that the classic diffraction models cannot effectively predict the loss of crossing bridges, although they work very well when the obstacles are solid. The predicted results of the CBG model (red line) and the measured received signal power (blue circles) have good agreement in all ten crossing bridges. The CBG model accurately describes the influence not only of the ICB but also of the CBGs.

Fig. 13 shows the comparisons on the path loss between the measurements and predicted results of the ICB model and the CBG model in validation scenario 1. It can be seen that the ICB model (green dashed line with circles) effectively predicts the extra loss of $Br1$, $Br2$, and $Br3$, because all of them are ICBs. The prediction performance of $Br4$, $Br6$, $Br7$, and $Br10$ is not so good but is still accepted, because these four bridges are the first bridge and the last bridge of the two groups, respectively. As shown in Fig. 2(e), the forward part of the related region of the first bridge and the rearward part of the related region of the last bridge are close to the case of the independent bridge. The obvious effect of the CBG appears on the middle bridges in a group. Therefore, clear deviations between the measurement and the ICB model appear in $Br5$, $Br8$, and $Br9$. These three bridges are the middle members of the two groups. Compared with the ICB model, the CBG model successfully describes the correlation of the members in the group, and therefore, it can be treated as a more general type of the ICB model.

Correspondingly, comparisons on the path loss between measurements and different models in validation scenarios 2 and 3 are shown in Figs. 14 and 15, respectively. The extended Hata model does not reflect the influence of crossing bridges, whereas the direct aid of the Deygout model that treats the

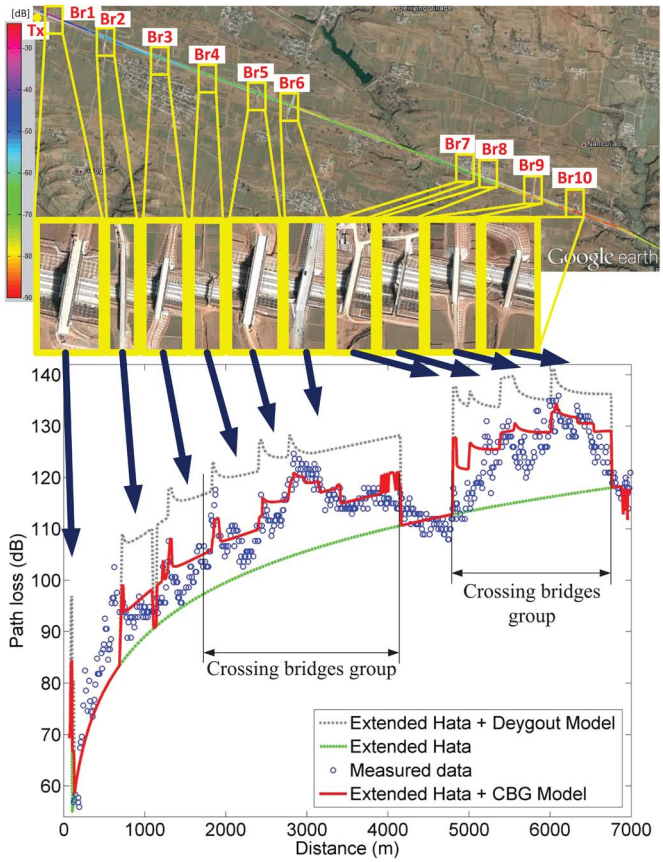

Fig. 12. Aerial view of validation scenario 1 and comparisons on the path loss between the measured result and different models.

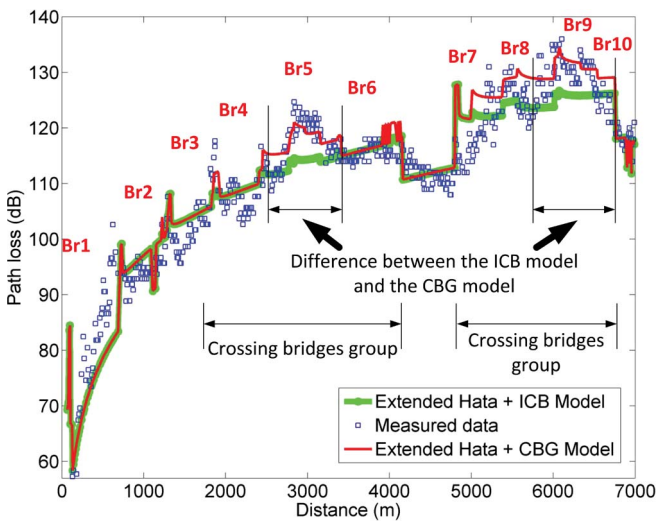

Fig. 13. Comparisons on the path loss between the measured and predicted results of the ICB model and the CBG model in validation scenario 1.

bridge as a solid obstruction leads to overestimation of the extra loss. The ICB model works well for the ICBs, even for the first and the last bridges in the CBGs. However, the ICB model does not consider the influence of the correlation of the members in the group, which have been effectively reflected by the CBG model.

The ME, Std, and RMSE between the measurements and predictions are given in Table VI. Overall, compared with the

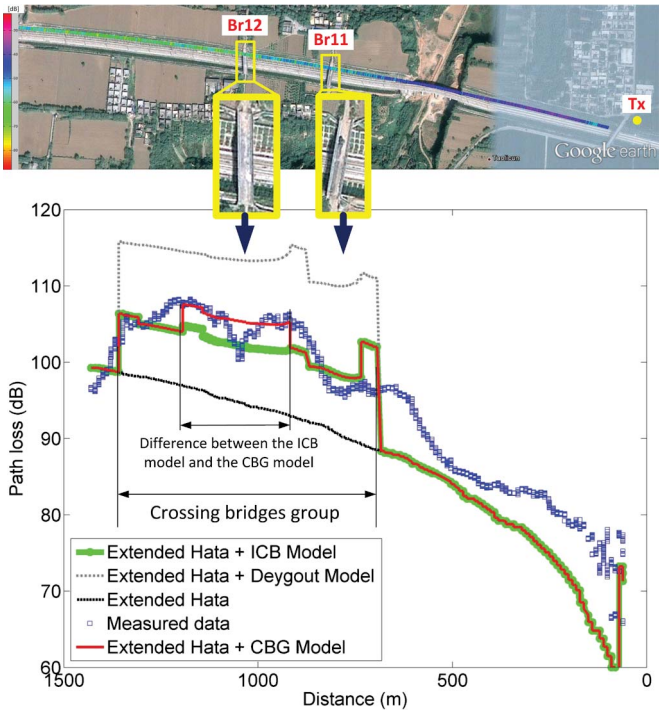

Fig. 14. Comparisons on the path loss between the measured result and different models in validation scenario 2. To accord with the aerial view, the path loss figure is flipped in the left/right direction of the x-axis.

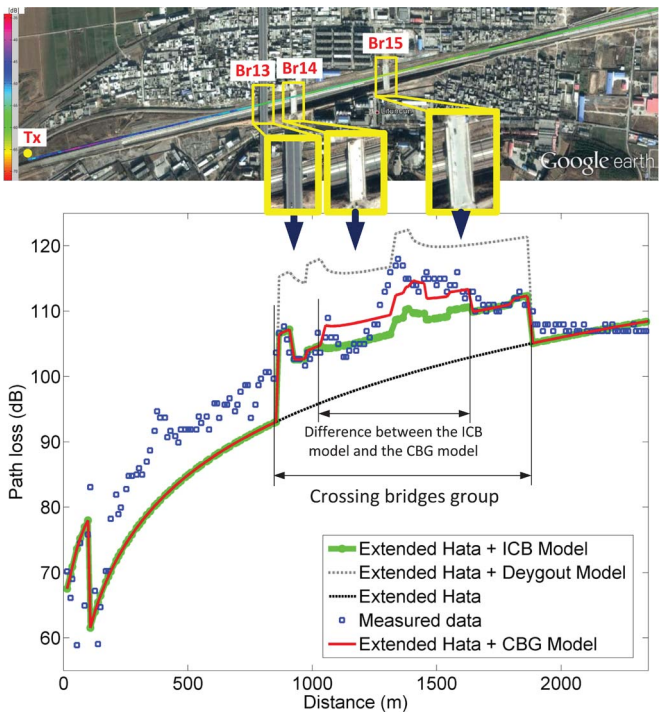

Fig. 15. Comparisons on the path loss between the measured result and different models in validation scenario 3.

extended Hata model and the Deygout model, the ICB model and the CBG model have considerable improvement in the accuracy of not only ME but also Std. The ME of the CBG model is close to 0 dB. This value of the ICB model is larger because of the existence of CBGs. Both models have good performance and are very easy to use.

VI. Conclusion

A group of 930-MHz measurements and two propagation loss models aiming to describe the influence of crossing bridges along a high-speed railway have been reported and presented for the first time. By considering the correlation of the influence of the crossing bridges and different mechanisms, the whole propagation process is investigated by four zones in the case of ICB.

- Zone A is the zone when the Rx is in the narrow space under the crossing bridge, but the LOS is still kept.
- Zone B is the zone when the Rx has passed the bridge, but the LOS is still kept.
- Zone C is the zone when the Rx has passed, but the LOS is blocked by the bridge.
- Zone D is the zone when the bridge is near the Tx, and the LOS is blocked before the Rx passes the bridge.

In the case of the CBG, two zones are defined.

- Zone A is the same as in the ICB case.
- Zone R is the sum of all the related regions (except Zone A) in the CBG.

First, based on extensive experimental results, propagation characteristics, including extra propagation loss, shadow fading, small-scale fading, and FD, have been measured, calculated, and summarized in a table. Our main results are summarized as follows.

- In the related regions, an extra loss of up to 24.00 dB due to the crossing bridges in Zone R has been observed. The mean values of the extra loss in all zones are from 5.96 to 14.18 dB. This indicates that the crossing bridge is a nonnegligible obstacle structure on propagation.
- FD values are considerably larger than the corresponding values in the existing high-speed-railway-related publications. Therefore, a larger fade margin is required in the link budget in the related regions of crossing bridges for an acceptably low system outage probability.
- The mean value of the K-factor in Zone A and Zone B is far smaller than in cuts and viaduct scenarios. This means that the crossing bridges strongly generate reflected and scattered waves so that the dominant part of the directed wave power is weakened even under the LOS condition.
- The mean value of the K-factor in Zone C and Zone D is small enough to allow description of the small-scale fading as Rayleigh. This implies that the channel in these two zones can be treated as the NLOS condition due to the blocking effect of the crossing bridge. This finding breaks the assumption that LOS is always available in high-speed rail scenarios.
- The Nakagami fading in Zone R reflects that the related bridges generate multiply scattered waves and different clusters of reflected waves.

Then, two empirical models (the ICB model and the CBG model) for the extra loss resulting from the crossing bridges are presented. The modeling approach treats the propagation situation of a crossing bridge as a combination of the open obstacle and the closed obstacle with different weight coefficients estimated from the measurement results in every propagation zone at 930 MHz.

TABLE VI
ME, STD, AND RMSE BETWEEN MEASUREMENTS AND PREDICTIONS

Model	Extended Hata + CBG Model	Extended Hata + ICB Model	Extended Hata + Deygout Model	Extended Hata
Validation Scenario 1				
ME (dB)	0.7	1.9	9.4	8.1
Std (dB)	3.4	4.0	6.4	4.9
RMSE (dB)	3.4	4.4	11.4	9.5
Validation Scenario 2				
ME (dB)	0.2	1.3	7.7	8.0
Std (dB)	3.0	3.1	5.4	3.4
RMSE (dB)	3.0	3.4	9.4	8.6
Validation Scenario 3				
ME (dB)	0.7	1.9	5.1	7.1
Std (dB)	2.6	2.9	5.7	5.0
RMSE (dB)	2.7	3.5	7.6	8.7
Overall (Mean Value)				
ME (dB)	0.5	1.7	7.4	7.7
Std (dB)	3.0	3.3	5.8	4.4
RMSE (dB)	3.0	3.7	9.5	8.9

By comparison with the measurements, the presented models have the ME close to 0 and achieve an improvement of more than 50% in the RMSE compared with the extended Hata model and the Deygout model. The ICB model and the CBG model compensate the limitations of the existing empirical models and effectively estimate the extra loss of crossing bridges. These models can be easily applied to the simulation and design of high-speed train control communications systems to substantially improve the fidelity of predicted path loss in those systems and produce more accurate simulation results overall.

REFERENCES

[1] H. Wei, Z. Zhong, K. Guan, and B. Ai, "Path loss models in viaduct and plain scenarios of the high-speed railway," in *Proc. CHINACOM*, Beijing, China, 2010, pp. 1–5.

[2] R. He, Z. Zhong, B. Ai, and J. Ding, "An empirical path loss model and fading analysis for high-speed railway viaduct scenarios," *IEEE Antennas Wireless Propag. Lett.*, vol. 10, pp. 808–812, Aug. 2011.

[3] H. Wei, Z. Zhong, L. Xiong, B. Ai, and R. He, "Study on the shadow fading characteristics in viaduct scenario of the high-speed railway," in *Proc. CHINACOM*, Beijing, China, 2011, pp. 1216–1220.

[4] R. He, Z. Zhong, B. Ai, and J. Ding, "Measurements and analysis of short-term fading behavior for high-speed rail viaduct scenario," in *Proc. IEEE ICC*, Ottawa, ON, Canada, 2012, pp. 4563–4567.

[5] R. He, Z. Zhong, B. Ai, and J. Ding, "Propagation measurements and analysis for high-speed railway cutting scenario," *Electron. Lett.*, vol. 47, no. 21, pp. 1167–1168, Oct. 2011.

[6] C. Briso, J. M. Cruz, and J. I. Alonso, "Measurements and modeling of distributed antenna systems in railway tunnels," *IEEE Trans Veh. Technol.*, vol. 56, no. 5, pp. 2870–2879, Sep. 2007.

[7] K. Guan, Z. Zhong, C. Briso, and J. I. Alonso, "Measurement of distributed antenna systems at 2.4 GHz in a realistic subway tunnel environment," *IEEE Trans Veh. Technol.*, vol. 61, no. 2, pp. 834–837, Feb. 2012.

[8] K. Guan, Z. Zhong, B. Ai, and C. Briso, "Propagation mechanism analysis before the break point inside tunnels," in *Proc. IEEE 74th Veh. Technol. Conf.*, San Francisco, CA, USA, 2011, pp. 1–5.

[9] K. Guan, Z. Zhong, B. Ai, and C. Briso, "Propagation mechanism modeling in the near region of circular tunnels," *IET Microw., Antennas Propag.*, vol. 6, no. 3, pp. 355–360, Apr. 2012.

[10] K. Guan, Z. Zhong, B. Ai, and C. Briso, "Modeling of the division point of different propagation mechanisms in the near-region within arched tunnels," *Wireless Pers. Commun.*, vol. 68, no. 3, pp. 489–505, Feb. 2012.

[11] K. Guan, Z. Zhong, B. Ai, R. He, Y. Li, and C. Briso, "Propagation mechanism modeling in the near-region of arbitrary cross-sectional tunnels," *Int. J. Antennas Propag.*, vol. 2012, pp. 183145-1–183145-11, Jan. 2012.

[12] K. Guan, Z. Zhong, B. Ai, and C. Briso, "Research of propagation characteristics of break point: Near zone and far zone under operational subway condition," in *Proc. IWCMC*, Caen, France, 2010, pp. 114–118.

[13] K. Guan, Z. Zhong, B. Ai, and C. Briso, "Measurement and modeling of subway near shadowing phenomenon," in *Proc. CHINACOM*, Beijing, China, 2010, pp. 1–5.

[14] K. Guan, Z. Zhong, B. Ai, and C. Briso, "Novel hybrid propagation model inside tunnels," in *Proc. IEEE 75th Veh. Technol. Conf.*, Yokohama, Japan, 2012, pp. 1–5.

[15] K. Guan, Z. Zhong, B. Ai, R. He, B. Chen, Y. Li, and C. Briso-Rodriguez, "Complete propagation modeling in tunnels," *IEEE Antennas Wireless Propag. Lett.*, vol. 12, pp. 741–744, Jun. 2013.

[16] K. Guan, Z. Zhong, B. Ai, R. He, B. Chen, Y. Li, and C. Briso, "Complete propagation model structure inside tunnels," *Progr. Electromagn. Res.*, vol. 141, pp. 711–726, Aug. 2013.

[17] K. Guan, Z. Zhong, B. Ai, R. He, and C. Briso, "Five-zone propagation model for large-size vehicles inside tunnels," *Progr. Electromagn. Res.*, vol. 138, pp. 389–405, Jul. 2013.

[18] L. Liu, J. Ch. Tao, H. Qiu, L. Chen, W. Yu, and Y. Dong, "Position-based modeling for wireless channel on high-speed railway under a viaduct at 2.35 GHz," *IEEE J. Sel. Areas Commun.*, vol. 30, no. 4, pp. 834–845, May 2012.

[19] K. Guan, Z. Zhong, and B. Ai, "Assessment of LTE-R using high speed railway channel model," in *Proc. 3rd Int. Conf. Commun. Mobile Comput.*, Qingdao, China, 2011, pp. 461–464.

[20] D. J. Cichon, T. Zwick, and W. Wiesbeck, "Radio link simulations in high-speed railway tunnels," in *Proc. Int. Conf. Antennas Propag.*, Eindhoven, The Netherlands, 1995, pp. 216–219.

[21] D. J. Cichon, T. Zwick, and W. Wiesbeck, "Ray optical modeling of wireless communications in high-speed railway tunnels," *Proc. IEEE 46th Veh. Technol. Conf.*, pp. 546–550, 1996.

[22] S. Knörzer, M. A. Baldauf, T. Fugen, and W. Wiesbeck, "Channel modelling for an OFDM train communications system including different antenna types," in *Proc. IEEE 64th Veh. Technol. Conf.*, Montreal, QC, Canada, 2006, pp. 1–5.

[23] S. Knörzer, M. A. Baldauf, T. Fugen, and W. Wiesbeck, "Channel analysis for an OFDM-MISO train communications system using different antennas," in *Proc. IEEE 66th Veh. Technol. Conf.*, Baltimore, MD, USA, 2007, pp. 809–813.

[24] J. Lu, G. Zhu, and C. Briso-Rodriguez, "Fading characteristics in the railway terrain cuttings," in *Proc. IEEE 73rd Veh. Technol. Conf.*, Budapest, Hungary, 2011, pp. 1–5.

[25] H. Hofestadt, "GSM-R: Global system for mobile radio communications for railways," in *Proc. Int. Conf. Electric Railways in a United Europe*, Amsterdam, Netherland, 1995, pp. 111–115. [Online]. Available: http://www.uic.asso.fr

[26] K. Guan, Z. Zhong, B. Ai, and T. Kürner, "Deterministic propagation modeling for the realistic high-speed railway environment," in *Proc. 77th IEEE Veh. Technol. Conf.*, Dresden, Germany, 2013, pp. 1–5.

[27] M. Werner, "Shuttle Radar Topography Mission (SRTM) mission overview," *Frequenz*, vol. 55, no. 3, pp. 75–79, Mar. 2001.

[28] W. C. Y. Lee, "Estimate of local average power of a mobile radio signal," *IEEE Trans Veh. Technol.*, vol. VT-34, no. 1, pp. 22–27, Feb. 1985.
[29] *Manual/Propagation Models/Extended Hata: Hata-and-Hata-SRD-implementation*, Eur. Commun. Office, Copenhagen, Denmark, 2011. [Online]. Available: http://tractool.seamcat.org/wiki/Manual/PropagationModels/ExtendedHata
[30] M. Prasad, K. Ratnamla, and P. K. Dalela, "Mobile communication measurements along railroads and model evaluations over eastern-Indian rural regions," *IEEE Antennas Propag. Mag.*, vol. 52, no. 5, pp. 131–141, Oct. 2010.
[31] M. V. S. N. Prasad, P. Dalela, and M. Chaitanya, "Experimental investigation of land mobile prediction methods and modeling of radio planning tool parameters along Indian rail road rural zones," *Int. J. Antennas Propag.*, vol. 2008, pp. 285763-1–285763-10, Jan. 2008.
[32] C. R. Garcia, A. Lehner, T. Strang and, and K. Frank, "Channel model for train to train communication using the 400 MHz band," in *Proc. IEEE 67th Veh. Technol. Conf.*, Singapore, 2008, pp. 3082–3086.
[33] COST Action 231. (1999). Digital mobile radio towards future generation systems, Eur. Commun., Brussels, Belgium, COST Action 231 Final Rep. EUR 18957, Tech. Rep., ch. 4.4.1. [Online]. Available: http://www.lx.it.pt/cost231/final_report.htm
[34] K. Schittkowski, "EASY-FIT: A software system for data fitting in dynamical Systems," *Struct. Multidisc. Optim.*, vol. 23, no. 2, pp. 153–169, Mar. 2002.
[35] G. L. Stüber, *Principles of Mobile Communication*. Boston, MA, USA: Kluwer, 1996, ch. 4.
[36] R. He, Z. Zhong, B. Ai, G. Wang, J. Ding, and A. F. Molisch, "Measurements and analysis of propagation channels in high-speed railway viaducts," *IEEE Trans. Wireless Comm.*, vol. 12, no. 2, pp. 794–805, Feb. 2013.
[37] R. He, Z. Zhong, B. Ai, J. Ding, Y. Yang, and A. F. Molisch, "Short-term fading behavior in high-speed railway cutting scenario: Measurements, analysis, and statistical models," *IEEE Trans. Antennas Propag.*, vol. 61, no. 4, pp. 2209–2222, Apr. 2013.
[38] S. Wyne, A. P. Singh, F. Tufvesson, and A. F. Molisch, "A statistical model for indoor office wireless sensor channels," *IEEE Trans. Wireless Commun.*, vol. 8, no. 8, pp. 4154–4164, Aug. 2009.
[39] U. G. Schuster and H. Bolcskei, "Ultrawideband channel modelling on the basis of information-theoretic criteria," *IEEE Trans. Wireless Commun.*, vol. 6, no. 7, pp. 2464–2475, Jul. 2007.
[40] X. H. Mao, Y. H. Lee, and B. C. Ng, "Statistical modeling of signal variation for propagation along a lift shaft," *IEEE Antennas Wireless Propag. Lett.*, vol. 9, pp. 752–755, Aug. 2010.
[41] P. M. Shankar, "A general statistical model for ultrasonic backscattering from tissues," *IEEE Trans. Ultrason., Ferroelectr., Freq. Control*, vol. 47, no. 3, pp. 727–736, May 2000.
[42] L. J. Greenstein, D. G. Michelson, and V. Erceg, "Moment-method estimation of the Ricean K-factor," *IEEE Commun. Lett.*, vol. 3, no. 6, pp. 175–176, Jun. 1999.
[43] A. Abdi, C. Tepedelenlioglu, M. Kaveh, and G. Giannakis, "On the estimation of the K parameter for the Rice fading distribution," *IEEE Commun. Lett.*, vol. 5, no. 3, pp. 92–94, Mar. 2001.
[44] S. Kozono, "Received signal-level characteristics in a wide-band mobile radio channel," *IEEE Trans. Veh. Technol.*, vol. 43, no. 3, pp. 480–486, Aug. 1994.
[45] J. Deygout, "Multiple knife-edge diffraction of microwaves," *IEEE Trans. Antennas Propag.*, vol. AP-14, no. 4, pp. 480–489, Jul. 1966.
[46] J. Epstein and D. W. Peterson, "An experimental study of wave propagation at 850 MC," *Proc. IRE*, vol. 41, no. 5, pp. 595–611, May 1953.
[47] H. Anderson, "New 2D physical EM propagation model selected," *IEEE Veh. Technol. Soc. News*, vol. 44, no. 3, pp. 15–22, Aug. 1997.
[48] R. Vauzelle, "A 3D diffraction model for VHF/UHF ranges," *Ann. Télécommun.*, vol. 51, no. 1, pp. 61–74, Jan. 1996.
[49] R. Saraiva Campos and L. Lovisolo, "A fast database correlation algorithm for localization of wireless network mobile nodes using coverage prediction and round trip delay," in *Proc. IEEE 69th Veh. Technol. Conf.*, Barcelona, Spain, 2009, pp. 1–5.
[50] A. Salieto, G. Roig, D. Gómez-Barquero, and N. Cardona, "Radio propagation models for DVB-H networks," in *Proc. Eur. Conf. Antennas Propag.*, Barcelona, Spain, 2010, pp. 1–5.
[51] A. Navarro, C. Ardila, and D. Mejıacute;a, "Some comparison between propagation models in Cost 2100 cali reference scenario," *S T Mag.*, vol. 7, no. 13, pp. 33–41, Aug. 2009, Cali.
[52] W. C. Y. Lee, *Mobile Communications Engineering*. New York, NY, USA: McGraw-Hill, 1985.
[53] K. L. Chee and T. Kürner, "Effect of terrain irregularities and clutter distribution on wave propagation at 3.5 GHz in suburban area," in *Proc. Eur. Conf. Antennas Propag.*, Barcelona, Spain, 2010, pp. 1–5.
[54] C. L. Giovaneli, "An analysis of simplified solutions for multiple knife-edge diffraction," *IEEE Trans. Antennas Propag.*, vol. AP-32, no. 3, pp. 297–301, Mar. 1984.
[55] J. H. Causebrook and B. Davies, "Tropospheric radio wave propagation over irregular terrain: The computation of field strength for UHF broadcasting," BBC Res. Dept., Salford, U.K., Rep. RD 1971/43, 1971.

Ke Guan (S'10) received the B.E. degree from Beijing Jiaotong University, Beijing, China, in 2006, where he is currently working toward the Ph.D. degree with the State Key Laboratory of Rail Traffic Control and Safety and the School of Electronic and Information Engineering.

In 2009, he was a Visiting Scholar with the Universidad Politecnica de Madrid, Madrid, Spain. From 2011 to 2013, he was a Research Scholar with the Institut für Nachrichtentechnik, Technische Universität Braunschweig, Braunschweig, Germany. He has authored/co-authored over 30 research papers in international journals and conferences. His current research interests include measurement and modeling of wireless propagation channels, high-speed railway communications, vehicle-to-x channel characterization, and indoor channel characterization for high-speed short-range systems including future terahertz communication systems.

Mr. Guan has been a member of the IC1004 initiative.

Zhangdui Zhong received the B.E. and Master's degrees from Beijing Jiaotong University, Beijing, China, in 1983 and 1988, respectively.

He is a Professor and an Advisor of Ph.D. candidates with Beijing Jiaotong University, Beijing, China. He is currently the Director of the School of Computer and Information Technology and a Chief Scientist with the State Key Laboratory of Rail Traffic Control and Safety, Beijing Jiaotong University. He is also the Director of the Innovative Research Team with the Ministry of Education and a Chief Scientist with the Ministry of Railways in China. He is an Executive Council Member of the Radio Association of China and a Deputy Director of the Radio Association of Beijing. He has authored/co-authored seven books and over 200 scientific research papers. He is the holder of five invention patents. His research interests include wireless communications for railways, control theory and techniques for railways, and Global System for Mobile Communications–Railway (GSM-R) systems. His research has been widely used in railway engineering, such as in the Qinghai–Xizang railway, the Datong–Qinhuangdao Heavy Haul railway, and in many high-speed railway lines of China.

Mr. Zhong received the MaoYiSheng Scientific Award of China, the ZhanTianYou Railway Honorary Award of China, and the Top 10 Science/Technology Achievements Award of Chinese Universities.

Bo Ai (M'00–SM'10) received the Master's and Ph.D. degrees from Xidian University, Xi'an, China, in 2002 and 2004, respectively.

In 2007, he graduated with great honors as a Excellent Postdoctoral Research Fellow from Tsinghua University, Beijing, China. He is currently a Professor and an Advisor of Ph.D. candidates with Beijing Jiaotong University. He is the Deputy Director of the State Key Laboratory of Rail Traffic Control and Safety. He has authored/co-authored six books and 140 scientific research papers. He is the holder of 26 invention patents. His current research interests include the research and applications of orthogonal frequency-division multiplexing techniques, high-power amplifier linearization techniques, radio propagation and channel modeling, and Global System for Mobile Communications–Railway (GSM-Railway) systems.

Dr. Ai is an Associate Editor for the IEEE TRANSACTIONS ON CONSUMER ELECTRONICS and an editorial committee member of *Wireless Personal Communications*. He is a Fellow of the Institution of Engineering and Technology.

Thomas Kürner (S'91–M'94–SM'01) received the Dipl.-Ing. degree in electrical engineering and the Dr.-Ing. degree from the Universität Karlsruhe, Karlsruhe, Germany, in 1990 and 1993, respectively.

From 1990 to 1994, he was with the Institut für Höchstfrequenztechnik und Elektronik, Universität Karlsruhe, working on wave propagation modeling, radio channel characterization, and radio network planning. From 1994 to 2003, he was with the radio network planning department at the headquarters of the GSM 1800 and Universal Mobile Telecommunications System (UMTS) operator E-Plus Mobilfunk GmbH & Co. KG, Düsseldorf, Germany, where he was the Team Manager, Radio Network Planning Support, responsible for radio network planning tools, algorithms, processes, and parameters. In 2012, he was a Guest Lecturer with Dublin City University, Dublin, Ireland. Since 2003, he has been a Professor of mobile radio systems with the Institut für Nachrichtentechnik, Technische Universität Braunschweig, Braunschweig, Germany. His fields of activity include propagation, traffic and mobility models for automatic planning of mobile radio networks, car-to-car communications, self-organizing Long-Term Evolution networks, indoor channel characterization for high-speed short-range systems including future terahertz communication systems, and multipath propagation in the Global Navigation Satellite System.

Dr. Kürner has been engaged in several international bodies, such as the ITU-R SG 3, UMTS Forum, Next Generation Mobile Networks Alliance, IEEE 802, and COST 231/273/259/2100/IC1004. He has participated in the following European projects: FP5-IST-MOMENTUM, FP7-ICT-SOCRATES, FP7-SME-GreenNets, and FP7-SEMAFOUR. He is currently the Chair of the IEEE802.15 Terahertz Interest Group (IGthz) and the Working Group Propagation of the European Association on Antennas and Propagation. He served as the Vice Chair of Propagation at the European Conference on Antennas and Propagation in 2007, 2009, and 2014. Since 2008, he has been an Associate Editor of the IEEE TRANSACTIONS ON VEHICULAR TECHNOLOGY.